

# Excitonic Instability in Ta<sub>2</sub>Pd<sub>3</sub>Te<sub>5</sub> monolayer

Jingyu Yao,<sup>1,2,\*</sup> Haohao Sheng,<sup>1,2,\*</sup> Ruihan Zhang,<sup>1,2</sup> Rongtian Pang,<sup>3</sup> Jin-Jian Zhou,<sup>3,†</sup>  
Quansheng Wu,<sup>1,2</sup> Hongming Weng,<sup>1,2</sup> Xi Dai,<sup>4</sup> Zhong Fang,<sup>1,2</sup> and Zhijun Wang<sup>1,2,‡</sup>

<sup>1</sup>Beijing National Laboratory for Condensed Matter Physics and Institute of Physics,  
Chinese Academy of Sciences, Beijing 100190, China

<sup>2</sup>University of Chinese Academy of Sciences, Beijing 100049, China

<sup>3</sup>Centre for Quantum Physics, Key Laboratory of Advanced Optoelectronic Quantum Architecture and Measurement (MOE),  
School of Physics, Beijing Institute of Technology, Beijing 100081, China

<sup>4</sup>Department of Physics, Hong Kong University of Science and Technology, Hong Kong 999077, China

(Dated: May 9, 2024)

By systematic theoretical calculations, we have revealed an excitonic insulator (EI) in a van der Waals (vdW) layered compound Ta<sub>2</sub>Pd<sub>3</sub>Te<sub>5</sub>. The interlayer binding energy in the vdW layered compound is 19.6 meV/Å<sup>2</sup>. The computed phonon spectrum suggests that the monolayer is dynamically stable without lattice distortion. The monolayer can be obtained by exfoliation or molecular-beam epitaxy. First-principles calculations show that the monolayer is a nearly zero-gap semiconductor with the modified Becke-Johnson functional. Due to the like symmetry of the band-edge states, the 2D polarization  $\alpha_{2D}$  would be finite as the band gap goes to zero, allowing for the EI state in the compound. Using the first-principles many-body perturbation theory, the *GW*-BSE calculation reveals that the exciton binding energy  $E_b$  is larger than the single-particle band gap  $E_g$ , indicating the excitonic instability. Our findings suggest that the Ta<sub>2</sub>Pd<sub>3</sub>Te<sub>5</sub> monolayer is an excitonic insulator without structural distortion.

*Introduction.* The excitonic insulator (EI) is an exotic ground state of narrow-gap semiconductors and/or semimetals, arising from the spontaneous condensation of electron-hole pairs bound by attractive Coulomb interactions [1–11]. The excitonic instability usually happens as the excitonic binding energy ( $E_b$ ) is larger than the single-particle band gap ( $E_g$ ). Due to the Coulomb screening effect [12], the EI candidates are rare in bulk compounds. In experiments, two kinds of bulk materials are considered as EIs, *e.g.*, 1T-TiSe<sub>2</sub> [13, 14] and Ta<sub>2</sub>NiSe<sub>5</sub> [15–17]. Due to the existence of the charge density wave transition or structural distortion, the origin of the phase transition in the two EI candidates is still under debate. The plasmon softening around the transition temperature was proposed to serve as the signature of the EI in 1T-TiSe<sub>2</sub> [18]. However, this result has not been supported by recent momentum-resolved high-resolution electron energy loss spectroscopy studies [19]. Although there is some compelling evidence for exciton condensation in artificial structures, such as InAs/GaSb quantum well [20] and MoSe<sub>2</sub>/WSe<sub>2</sub> bilayers [21, 22], the experimental confirmation for the EI state in real materials remains unsolved.

On the other hand, lower dimensionality can significantly weaken the screening effect and result in a larger  $E_b$ . However,  $E_b$  usually shows a strong dependence on  $E_g$ , *i.e.*,  $E_b \sim E_g/4$  in two-dimensional (2D) materials [23]. To break this dependence, one strategy is to seek dipole-forbidden transitions near the band edges [24–27]. Thus, some 2D materials are theoretically predicted to

be EI candidates, such as GaAs [24], AlSb [28], AsO [27], and Mo<sub>2</sub>MC<sub>2</sub>F<sub>2</sub> ( $M = \text{Ti, Zr, Hf}$ ) [29]. Interestingly, some quantum spin Hall insulators with large band inversion can result in the same-parity band-edge states. The topological EI can be achieved in such systems [27, 29]. However, these 2D EI candidates still need experimental confirmation.

In this work, we demonstrate that Ta<sub>2</sub>Pd<sub>3</sub>Te<sub>5</sub> monolayer shows the excitonic instability by systematic theoretical calculations. The first-principles calculations with modified Becke-Johnson functional suggest that the monolayer has a nearly zero band gap and the band-edge states have like symmetry of  $C_{2z}$  rotation. Upon applying the strains, the polarization  $\alpha_{2D}$  shows little response to the reduction of  $E_g$ . The band gap was obtained by the *GW* calculation with  $E_g = 130$  meV. To calculate  $E_b$ , we performed the first-principles *GW*-BSE calculations. The obtained  $E_b = 633$  meV is larger than the  $E_g$ , indicating excitonic instability. The strain-dependent calculations show that the  $E_b$  remains almost unchanged across a wide range of strain. Unlike 1T-TiSe<sub>2</sub> and Ta<sub>2</sub>NiSe<sub>5</sub>, no structural instability is found in the phonon spectrum of this material. Our findings suggest that the Ta<sub>2</sub>Pd<sub>3</sub>Te<sub>5</sub> monolayer is an excitonic insulator without structural distortion.

*Calculation methods.* First-principles calculations were performed within the framework of density functional theory (DFT) using the projector augmented wave (PAW) method [30, 31], as implemented in Vienna *ab initio* simulation package (VASP) [32, 33].  $20 \times 4 \times 1$   $k$ -point sampling grids were used, and the cut-off energy for plane wave expansion was 500 eV. Phonon spectra were obtained with the finite-difference method using a  $2 \times 2 \times 1$  supercell, as implemented in the Phonopy package [34]. Considering that the Perdew-Burke

\* These authors contributed equally to this work.

† jjzhou@bit.edu.cn

‡ wzj@iphy.ac.cn

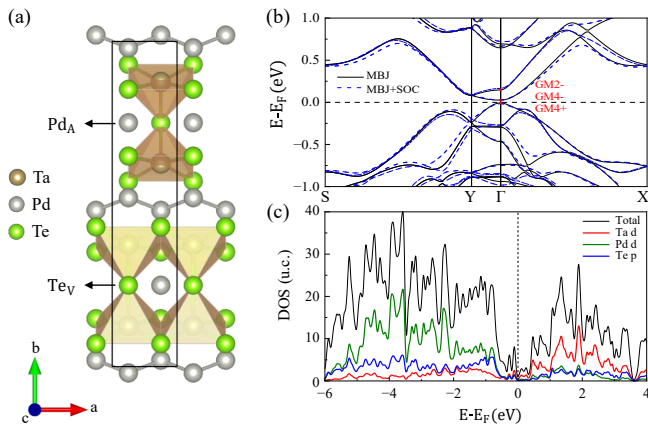


FIG. 1. The crystal structure and band structures of the  $\text{Ta}_2\text{Pd}_3\text{Te}_5$  monolayer. (a) Crystal structure of the monolayer. (b) MBJ band structures with and without spin-orbit coupling. The highest VB is labeled by  $v_1$ , while the first and second lowest CBs are labeled by  $c_1$  and  $c_2$ , respectively. (c) Total and partial DOS for Ta  $d$ , Pd  $d$ , and Te  $p$  orbitals.

Ernzerhof (PBE) exchange correlation functional [35] underestimates the band gap, the band structures were obtained by using the modified Becke-Johnson (MBJ) functional [36, 37]. Moreover, to compute the binding energy  $E_b$  [38–42], the first-principles many-body  $GW$ -BSE calculations on top of the PBE band structure were performed with the Coulomb cutoff technique in the Yambo package [43, 44]. Quasi-particle (QP) corrections in  $GW$  calculations are  $k$ -point and band dependent. The same  $k$ -point grid, and 4 Ry cutoff were used to calculate the dielectric function matrix. The kinetic energy cutoff of 70 Ry was used for the evaluation of the exchange part of the self-energy. Achieving convergence of the  $G_0W_0$  band gap involves employing 300 bands along with an extrapolar correction scheme [45]. To speed up  $k$ -point convergence, we employ a combination of Monte Carlo integration and an interpolation scheme capable of representing the screened potential between the calculated grid points [46]. One valence band (VB) and two conduction bands (CBs) were included to build the BSE Hamiltonian. For comparison, we have performed the BSE calculations on top of the PBE and MBJ band structures, to check the band gap dependence of  $E_b$ . In the MBJ-BSE calculations, the scissor operator, which applies the gap correction from PBE to MBJ at the  $\Gamma$  point, is used to correct the QP energies, and is introduced into both the response function and the diagonal part of the BSE kernel.

**Band structure and Density of states.** The van der Waals (vdW) layered compound  $\text{Ta}_2\text{Pd}_3\text{Te}_5$  crystallizes in an orthorhombic structure with two vdW layers in a unit cell [47]. The PBE calculations show that the interlayer binding energy is  $19.6 \text{ meV}/\text{\AA}^2$  in our previous work [47]; thus, its monolayer/thin-film structures could be readily obtained by exfoliation. Fig. 1(a) shows its monolayer structure with the space group  $Pmmn$  (#59).

The inversion and two mirror symmetries ( $M_x, M_y$ ) are respected. The quasi-1D chains are along the  $x$  direction. The phonon spectrum of the monolayer is obtained in Fig. 2(d). No phonon mode with negative frequency in the phonon spectrum suggests that the monolayer is dynamically stable.

The MBJ band structure along the high-symmetry lines is presented in Fig. 1(b). The irreducible representations (irreps) of the two band-edge states are computed as GM4+ ( $v_1$  band) and GM4– ( $c_1$  band) by the **IRVSP** program [48, 49]. Thus, we define the band gap at  $\Gamma$  by  $E_g \equiv E_{\text{GM4-}} - E_{\text{GM4+}} = 33 \text{ meV}$ , resulting in a nearly zero-gap semiconductor. The spin-orbit coupling (SOC) does not change the band structure at all, but slightly enlarges the band gap to 44 meV. This is because the CBs primarily originate from the Ta- $d_{z^2}$  orbitals with  $J_z = 0$ , which have little SOC effect. Hereafter, the SOC is neglected in the following calculations. Additionally, the symmetry eigenvalues of the three lowest energy bands are presented in Table I. They show that the two band-edge bands both have the like symmetry of  $C_{2z}$  rotation, although they are of different parity. Thus, the 2D polarizability  $\alpha_{2D}$  can still be finite when  $E_g \rightarrow 0$ , breaking the strong dependence and allowing for the EI candidate with  $E_b > E_g$ . Furthermore, due to the significantly enhanced  $E_b$  in lower dimensions, the  $\text{Ta}_2\text{Pd}_3\text{Te}_5$  layers with the quasi-1D structure present a promising opportunity to realize an intrinsic EI.

The total and partial densities of states (DOS) are plotted in Fig. 1(c). The results show that the CBs are mainly from Ta  $d$  states, while the VBs are mainly from Pd  $d$  states. The Te  $p$  states have strong hybridization with them, and have certain contributions both below and above the Fermi level ( $E_F$ ). In particular, the orbital-resolved band structures in Figs. 4(a-b) show that the CBs are contributed by Ta  $d_{z^2}$  states, while the VBs are formed by the hybridization of Pd<sub>A</sub>  $d_{xz}$  and Te<sub>V</sub>  $p_x$  states [50]. The related bonds are  $d_{\text{Ta-Pd}_A} = 2.99 \text{ \AA}$  and  $d_{\text{Ta-Te}_V} = 2.82 \text{ \AA}$ , respectively. Although these bond hoppings are allowed, the CB and VB states do not mix on the line  $Y\Gamma$  due to the different  $M_x$  eigenvalues. The interaction between Ta- $d$  electrons and the Pd- $d$ /Te- $p$  holes may be crucial to the formation of the EI state in the compound.

**Evolution of  $\alpha_{2D}$  under strain.** As we know, the band gap of this material is sensitive to the strain [47]. Figs. 2(a,b) show the MBJ band structures with uniaxial strains along  $y$ . When the system is compressed by 1% in Fig. 2(a), the gap increases to 87 meV; in contrast, it

TABLE I. The symmetry of the highest VB ( $v_1$  band) and the lowest two CBs ( $c_1$  and  $c_2$  bands) at  $\Gamma$ .

band	irrep	$C_{2z}$	$M_y$
$v_1$	GM4+	-1	+1
$c_1$	GM4-	-1	-1
$c_2$	GM2-	+1	+1

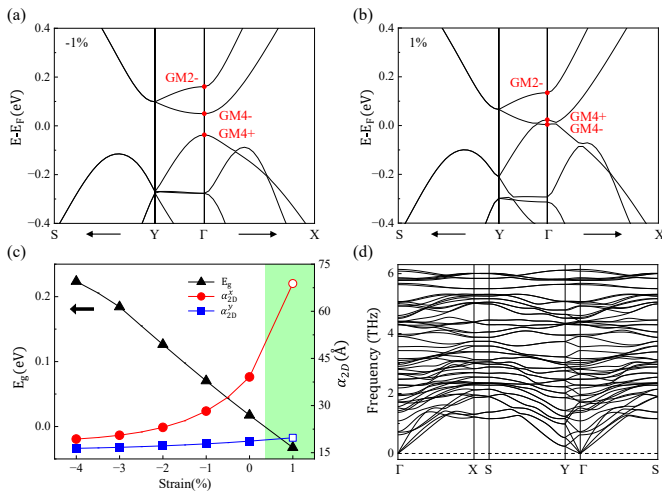


FIG. 2. The evolution of band structures and polarization  $\alpha_{2D}$  under uniaxial strain  $\eta$ ,  $b = (1 + \eta)b_0$ . (a,b) The band structure with uniaxial strains  $\eta = -1\%$  (a) and  $+1\%$  (b), respectively. (c)  $E_g$  and  $\alpha_{2D}$  under different uniaxial strains. (d) The phonon spectrum of  $\text{Ta}_2\text{Pd}_3\text{Te}_5$  monolayer. There is no imaginary frequency phonon mode.

becomes metallic under tensile strain in Fig. 2(b). The 2D polarization, denoted as  $\alpha_{2D}^{x/y}$ , is calculated with the formula  $\alpha_{2D}^{x/y} = c_0 \frac{\varepsilon^{xx/yy} - 1}{4\pi}$ , where  $c_0$  is the thickness of the vacuum in the  $z$  direction. The  $\varepsilon^{xx/yy}$  represents the  $xx/yy$  components of the macroscopic static dielectric tensor, which is computed with the random phase approximation and considering the local field effects, as implemented in VASP.

In Fig. 2(c), we plot  $E_g$  and 2D polarization  $\alpha_{2D}^{x/y}$  as a function of the uniaxial strain. In the positive gap range, both show a weak dependence on the reduction of the band gap. Especially,  $\alpha_{2D}^y$  is almost unchanged. The weak dependence of  $\alpha_{2D}^x$  is attributed to the transition between the  $v_1$  band and the second lowest CB ( $c_2$  band). The symmetry eigenvalues at  $\Gamma$  yield  $\langle c_2 | \nabla_{k_y} | v_1 \rangle = 0$  and  $\langle c_2 | \nabla_{k_x} | v_1 \rangle \neq 0$ , which have been confirmed numerically [51]. As aforementioned, the band-edge transition between  $c_1$  and  $v_1$  bands is forbidden due to the twofold rotation. This indicates the decoupling between  $E_g$  and  $E_b$  in this material with band-edge states of the same  $C_{2z}$  symmetry.

*Stable phonon spectrum.* In previous studies [52, 53], the phonon spectra of previous EI candidates  $1T\text{-TiSe}_2$  and  $\text{Ta}_2\text{NiSe}_5$  show the structural instability with imaginary frequency phonon modes. Whether the charge-density-wave transition in  $1T\text{-TiSe}_2$  comes from the Jahn-Teller mechanism or from the excitonic instability has plagued the EI community for decades. Additionally, as indicated by the imaginary frequency mode, the structure distortion of  $\text{Ta}_2\text{NiSe}_5$  from  $Cmcm$  (SG #63) to  $C2/c$  (SG #15) occurs at 328 K [54–56], accompanied by a metal-to-insulator transition even in the single-particle band structure calculations.

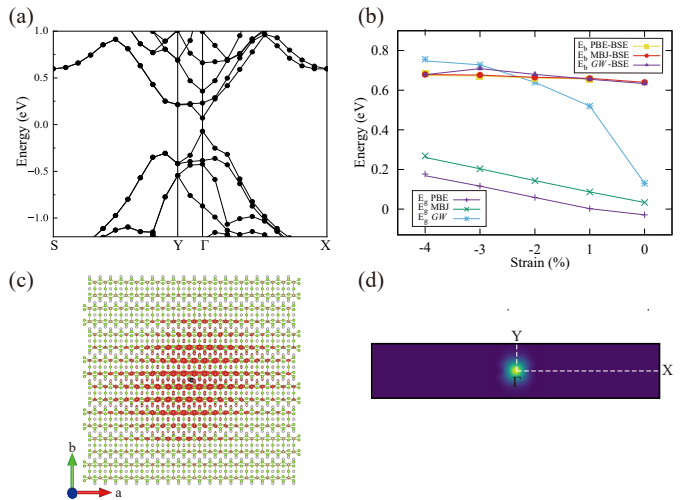


FIG. 3. (a) The  $G_0W_0$  band structure. (b) Strain dependence of  $E_g$  and  $E_b$  with different methods (PBE, MBJ, and GW). The GW-BSE results strongly show an intrinsic EI with  $E_b > E_g$  at  $\eta > -2\%$ . (c) Exciton wavefunction square modulus, as obtained from the Bethe-Salpeter equation (GW-BSE). The contour plot (red) is the probability density of locating the bound electron once the hole position is fixed (black dot). The figure contains 20 and 4 unit cells in the  $x$  and  $y$  directions, respectively. We note that it is well-localized around the hole. (d) Exciton wavefunction square modulus in reciprocal space. The exciton probability weight is localized around the  $\Gamma$  point.

However, our calculation shows that there is no imaginary frequency on the phonon spectrum of  $\text{Ta}_2\text{Pd}_3\text{Te}_5$  monolayer in Fig. 2(d). Even if we start from some degree of distortion, the relaxation still yields the  $Pm\bar{m}n$  symmetry structure. The phonon spectrum of the bulk  $\text{Ta}_2\text{Pd}_3\text{Te}_5$  also does not show any imaginary frequency modes, quite different from the previous two examples. Experimentally, no structural distortion is found in the X-Ray diffraction data [47]. Therefore,  $\text{Ta}_2\text{Pd}_3\text{Te}_5$  inherently excludes Jahn-Teller-like instabilities, consequently avoiding the confusion of  $1T\text{-TiSe}_2$  or  $\text{Ta}_2\text{NiSe}_5$ . However, the lack of a structural signal usually poses challenges for identifying an EI phase transition. The symmetry breaking of the EI phase transition could be weakly coupled to the lattice structure, which needs high-resolution measurements, such as electron diffraction.

*Binding energy and GW-BSE calculations.* In order to investigate the excitonic instability, we carry out many-body GW calculations in a single-shot scheme ( $G_0W_0$ ). The GW band structure in Fig. 3(a) does not change significantly from the MBJ one except that the  $E_g$  changes from 33 meV to 130 meV. The first-principles GW-BSE calculation shows that the  $E_b = 633$  meV. This  $E_b$  value exceeds the GW band gap  $E_g$ , indicating that it is an excitonic insulator in the  $\text{Ta}_2\text{Pd}_3\text{Te}_5$  monolayer. The lowest-energy exciton is non-degenerate, and its strength indicates that this exciton is comparatively bright. The lowest-energy exciton probability weight in momentum space is localized around the  $\Gamma$  point in

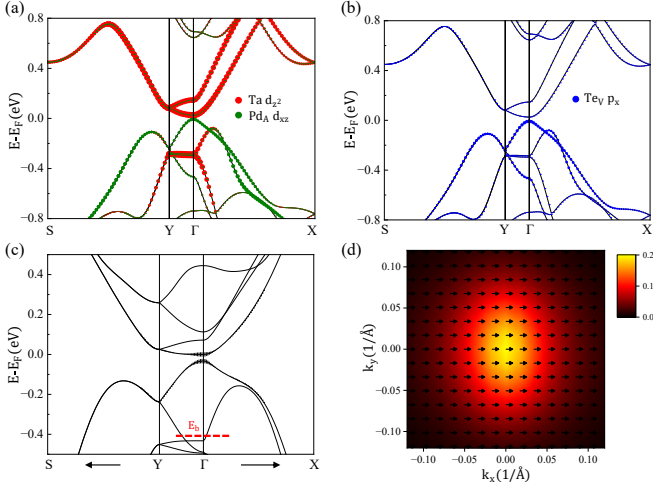


FIG. 4. (a-b) The orbital-resolved MBJ band structures for Ta  $d_{z^2}$ , Pd<sub>A</sub>  $d_{xz}$ , and Te<sub>V</sub>  $p_x$  orbitals. (c) The band structure of the effective TB model. The band spread corresponds to the contribution of a particular electron-hole transition to the lowest-energy exciton. (d) Absolute values (color) and phase angles (arrows) of the lowest-energy exciton wavefunction.

Fig. 3(d). The lowest-energy exciton wavefunction in real space is shown in Fig. 3(c) as the conditional probability of finding a bound electron (red), provided the hole position is fixed (black dot). The electron is well-localized around the hole, within a radius of 30 Å.

In order to check the band gap dependence of  $E_b$ , we also performed the *GW*-BSE calculations under uniaxial compressive strains. On the other hand, since different band gaps are obtained with different methods, we have also performed the BSE calculations to obtain the  $E_b$  on top of the PBE and MBJ calculations with positive band gaps. The results are presented in Fig. 3(b), which shows the  $E_b$  as a function of the compressive strains with different methods. We find that the obtained  $E_b$  is almost unchanged, although the  $E_g$  changes for different strains and methods. We conclude that the  $E_b$  in the Ta<sub>2</sub>Pd<sub>3</sub>Te<sub>5</sub> monolayer shows little response to the change of  $E_g$ . We attribute it to the unique wavefunctions of the conduction and valence states, which originate from Ta and Pd/Te atoms, respectively. In the *GW*-BSE calculations, the obtained  $E_b$  exceeds the  $E_g$  at  $\eta > -2\%$ , indicating the EI instability in the Ta<sub>2</sub>Pd<sub>3</sub>Te<sub>5</sub> monolayer.

*Effective model and symmetry analysis.* From the orbital-resolved band structures in Figs. 4(a-b), we find the valence bands are mainly formed the Pd<sub>A</sub>  $d_{xz}$  states, hybridizing with the Te  $p_x$  states (especially Te<sub>V</sub>). The CBs are from the Ta  $d_{z^2}$  states, which do not hybridize with the valence bands along the Y- $\Gamma$  line. Accordingly, we construct a sixteen-band Wannier-based tight-binding (TB) Hamiltonian, extracted from the DFT calculations by using Wannier90 package [57]. Under the basis of these Wannier orbitals  $\{|\alpha\mathbf{k}\rangle\}$ , the eigenvalues and eigenstates of  $H_{TB}$  yield  $\hat{H}_{TB}(\mathbf{k})|b\mathbf{k}\rangle = E_b(\mathbf{k})|b\mathbf{k}\rangle$ . On top of the TB model in Fig. 4(c), we have solved the model BSE

to find the collective modes. The BSE reads [58–60],

$$(\Omega_S - E_c(\mathbf{k}) + E_v(\mathbf{k}))A_{cv}^S(\mathbf{k}) = \sum_{c'v'\mathbf{k}'} \mathcal{K}_{c'v'\mathbf{k}'}^{cv\mathbf{k}} A_{c'v'}^S(\mathbf{k}'), \quad (1)$$

where  $c, v$  are the labels of conduction and valence bands,  $\Omega_S$  is the energy of exciton eigenstates,  $|S\rangle \equiv \sum_{cv\mathbf{k}} A_{cv}^S(\mathbf{k}) \hat{c}_{c\mathbf{k}}^\dagger \hat{c}_{v\mathbf{k}} |0\rangle$ , and  $|0\rangle$  is the non-interacting ground state. The kernel consists of the direct part  $\mathcal{K}^d$  and the exchange part  $\mathcal{K}^x$

$$\begin{aligned} \mathcal{K}_{c'v'\mathbf{k}'}^{cv\mathbf{k}} &= \mathcal{K}_{c'v'\mathbf{k}'}^{d^{cv\mathbf{k}}} + \mathcal{K}_{c'v'\mathbf{k}'}^{x^{cv\mathbf{k}}}, \\ \mathcal{K}_{c'v'\mathbf{k}'}^{x^{cv\mathbf{k}}} &= -V f_{cv}(\mathbf{k}, \mathbf{k}') f_{v'c'}(\mathbf{k}', \mathbf{k}'), \\ \mathcal{K}_{c'v'\mathbf{k}'}^{d^{cv\mathbf{k}}} &= -W(\mathbf{k} - \mathbf{k}') f_{cc'}(\mathbf{k}, \mathbf{k}') f_{v'v}(\mathbf{k}', \mathbf{k}). \end{aligned} \quad (2)$$

Here  $V$  is the bare Coulomb potential, and  $W(\mathbf{q}) = 2\pi e^2 / [S|\mathbf{q}|(1 + \alpha_{2D}|\mathbf{q}|)]$  is the screened Coulomb potential [61, 62], where  $S$  is the system area and the computed 2D polarization  $\alpha_{2D} = 17.854$  Å is used. We define  $f_{b_1 b_2}(\mathbf{k}, \mathbf{k}') \equiv \sum_{\alpha} \langle b_1 \mathbf{k} | \alpha \mathbf{k} \rangle \langle \alpha \mathbf{k}' | b_2 \mathbf{k}' \rangle$ ,  $b_1, b_2 \in \{c, v\}$ . Since  $f_{cv}(\mathbf{k}, \mathbf{k}) = 0$ ,  $\mathcal{K}_{cv\mathbf{k}, c'v'\mathbf{k}'}^x = 0$ . By solving Eq. (1), one can obtain the discrete excitonic binding energies with electron-hole attractive Coulomb interactions. The lowest excitonic binding energy is depicted in Fig. 4(c), which is larger than the band gap. The 1s-like exciton wavefunction is given in Fig. 4(d) in the vicinity of the  $\Gamma$  point, where colors and arrows indicate the distribution of absolute values and phase angles, respectively. Although the  $E_b$  is smaller than the DFT result, the distribution of the exciton is consistent with the DFT one. In the Bose-Einstein condensation (BEC) state of this exciton, the expectation value can be  $\rho_{cv}(\mathbf{k}) = \langle a_{c,\mathbf{k}}^\dagger a_{v,\mathbf{k}} \rangle = \text{const.}$ , which is the excitonic order parameter in the Hartree-Fock approximation. In the Hartree-Fock mean-field Hamiltonian ( $H = H_{TB} + H_{MF}$ ), the pairing term  $H_{MF} = \rho_{cv}(\mathbf{k}) a_{v,\mathbf{k}}^\dagger a_{c,\mathbf{k}} + c.c.$  is introduced, where  $a_{v,\mathbf{k}}^\dagger$  and  $a_{c,\mathbf{k}}$  are band electron creation and annihilation operators. As the VB and the CB belong to GM4+ and GM4− irreps respectively, which have different symmetry eigenvalues of spatial inversion and mirror symmetries, the exciton pairing term breaks spatial inversion and all mirror symmetries in the excitonic BEC state.

*Discussion.* In this work, we demonstrate that the Ta<sub>2</sub>Pd<sub>3</sub>Te<sub>5</sub> monolayer is an excitonic insulator by first-principles *GW*-BSE calculations. In the single-particle picture, the MBJ calculation shows that the monolayer is a nearly zero-gap semiconductor. The low-energy states at  $\Gamma$  have the same  $C_{2z}$  symmetry eigenvalue, making the band-edge transitions forbidden and keeping the  $\alpha_{2D}$  finite as  $E_g \rightarrow 0$ . By applying the uniaxial strain, the  $\alpha_{2D}$  shows little response to the reduction of  $E_g$ . The *GW* band gap is calculated to be 130 meV. The  $E_b = 633$  meV is obtained by performing the *GW*-BSE calculations in Yambo, indicating an intrinsic EI with  $E_b > E_g$ . By investigating the strain effect, we find that the strong excitonic instability is robust against small strains. In conclusion, we predict that the Ta<sub>2</sub>Pd<sub>3</sub>Te<sub>5</sub> monolayer is

an excitonic insulator, which is very promising in experiments.

In the  $\text{Ta}_2\text{Pd}_3\text{Te}_5$  bulk, the band-edge states at  $\Gamma$  are of the same parity, making transitions between them forbidden. In addition, this material possesses several advantages for the formation of an EI phase. To begin with, in the series of the  $A_2M_3X_5$  ( $A = \text{Ta}, \text{Nb}$ ;  $M = \text{Pd}, \text{Ni}$ ;  $X = \text{Se}, \text{Te}$ ) family, the band gap is modified by chemical doping. Different from the small gap semiconductor  $\text{Ta}_2\text{Ni}_3\text{Te}_5$  with higher-order topology [50] and the metallic compound  $\text{Nb}_2\text{Pd}_3\text{Te}_5$  with superconductivity [63], the  $\text{Ta}_2\text{Pd}_3\text{Te}_5$  is a nearly zero-gap semiconductor, exhibiting strong EI instability. Then, it is a vdW layered compound with 1D chains and strong anisotropy, where the screening effect is relatively weak, resulting in a large excitonic binding energy. Next, the chemical potential of the crystals is right in the tiny band gap in

experiments, showing the ideal balance of the electrons and holes for excitonic condensation. Finally, the layered compound is easy to exfoliate, and its properties can be readily tuned by the gate voltage. Therefore, the EI state may survive in the few-layer flake and bulk samples.

*Acknowledgements.* We thank Xinzheng Li, Huaiyuan Yang, Yuelin Shao and Xinguo Ren for helpful discussions. This work was supported by the National Natural Science Foundation of China (Grants No. 11974395, No. 12188101), the Strategic Priority Research Program of Chinese Academy of Sciences (Grant No. XDB33000000), National Key R&D Program of Chain (Grants No. 2022YFA1403800 and No. 2022YFA1403400), and the Center for Materials Genome.

*Note added.* In the preparation of this work, we notice the related works in experiment [64–66].

- 
- [1] D. Jérôme, T. M. Rice, and W. Kohn, *Phys. Rev.* **158**, 462 (1967).
- [2] Y.-P. Shim and A. H. MacDonald, *Phys. Rev. B* **79**, 235329 (2009).
- [3] B. Sun, W. Zhao, T. Palomaki, Z. Fei, E. Runburg, P. Malinowski, X. Huang, J. Cenker, Y.-T. Cui, J.-H. Chu, X. Xu, S. S. Ataei, D. Varsano, M. Palummo, E. Molinari, M. Rontani, and D. H. Cobden, *Nature Physics* **18**, 94 (2022).
- [4] Y. Jia, P. Wang, C.-L. Chiu, Z. Song, G. Yu, B. Jäck, S. Lei, S. Klemenz, F. A. Cevallos, M. Onyszczyk, N. Fishchenko, X. Liu, G. Farahi, F. Xie, Y. Xu, K. Watanabe, T. Taniguchi, B. A. Bernevig, R. J. Cava, L. M. Schoop, A. Yazdani, and S. Wu, *Nature Physics* **18**, 87 (2022).
- [5] L. Kong, R. Shindou, and Y. Zhang, *Phys. Rev. B* **106**, 235145 (2022).
- [6] Q. Gao, Y.-h. Chan, Y. Wang, H. Zhang, P. Jinxu, S. Cui, Y. Yang, Z. Liu, D. Shen, Z. Sun, J. Jiang, T. C. Chiang, and P. Chen, *Nature Communications* **14**, 994 (2023).
- [7] Y. Song, C. Jia, H. Xiong, B. Wang, Z. Jiang, K. Huang, J. Hwang, Z. Li, C. Hwang, Z. Liu, D. Shen, J. A. Sobota, P. Kirchmann, J. Xue, T. P. Devereaux, S.-K. Mo, Z.-X. Shen, and S. Tang, *Nature Communications* **14**, 1116 (2023).
- [8] R. Wang, T. A. Sedrakyan, B. Wang, L. Du, and R.-R. Du, *Nature* **619**, 57 (2023).
- [9] D. I. Pikulin and T. Hyart, *Phys. Rev. Lett.* **112**, 176403 (2014).
- [10] J. Ma, S. Nie, X. Gui, M. Naamneh, J. Jandke, C. Xi, J. Zhang, T. Shang, Y. Xiong, I. Kapon, N. Kumar, Y. Soh, D. Gosálbez-Martínez, O. V. Yazyev, W. Fan, H. Hübener, U. D. Giovannini, N. C. Plumb, M. Radovic, M. A. Sentef, W. Xie, Z. Wang, C. Mudry, M. Müller, and M. Shi, *Nature Materials* **21**, 423 (2022).
- [11] Y. Shao and X. Dai, (2023), [arXiv:2302.07543](https://arxiv.org/abs/2302.07543) [cond-mat.mes-hall].
- [12] M. Rohlfing, P. Krüger, and J. Pollmann, *Phys. Rev. B* **48**, 17791 (1993).
- [13] H. Cercellier, C. Monney, F. Clerc, C. Battaglia, L. Despont, M. G. Garnier, H. Beck, P. Aebi, L. Patthey, H. Berger, and L. Forró, *Phys. Rev. Lett.* **99**, 146403 (2007).
- [14] C. Monney, H. Cercellier, F. Clerc, C. Battaglia, E. F. Schwier, C. Didiot, M. G. Garnier, H. Beck, P. Aebi, H. Berger, L. Forró, and L. Patthey, *Phys. Rev. B* **79**, 045116 (2009).
- [15] Y. Wakisaka, T. Sudayama, K. Takubo, T. Mizokawa, M. Arita, H. Namatame, M. Taniguchi, N. Katayama, M. Nohara, and H. Takagi, *Phys. Rev. Lett.* **103**, 026402 (2009).
- [16] Y. Wakisaka, T. Sudayama, K. Takubo, T. Mizokawa, N. L. Saini, M. Arita, H. Namatame, M. Taniguchi, N. Katayama, M. Nohara, and H. Takagi, *Journal of Superconductivity and Novel Magnetism* **25**, 1231 (2012).
- [17] G. Mazza, M. Rösner, L. Windgätter, S. Latini, H. Hübener, A. J. Millis, A. Rubio, and A. Georges, *Phys. Rev. Lett.* **124**, 197601 (2020).
- [18] A. Kogar, M. S. Rak, S. Vig, A. A. Husain, F. Flicker, Y. I. Joe, L. Venema, G. J. MacDougall, T. C. Chiang, E. Fradkin, J. van Wezel, and P. Abbamonte, *Science* **358**, 1314 (2017).
- [19] Z. Lin, C. Wang, A. Balassis, J. P. Echeverry, A. S. Vasenko, V. M. Silkin, E. V. Chulkov, Y. Shi, J. Zhang, J. Guo, and X. Zhu, *Phys. Rev. Lett.* **129**, 187601 (2022).
- [20] D. Lingjie, L. Xinwei, L. Wenkai, S. Gerard, C. Kai, K. Junichiro, and D. Rui-Rui, *Nature Communications* **8**, 1971 (2017).
- [21] Z. Wang, D. A. Rhodes, K. Watanabe, T. Taniguchi, J. C. Hone, J. Shan, and K. F. Mak, *Nature* **574**, 76 (2019).
- [22] M. Troue, J. Figueiredo, L. Sigl, C. Paspalides, M. Katzer, T. Taniguchi, K. Watanabe, M. Selig, A. Knorr, U. Wurstbauer, and A. W. Holleitner, *Phys. Rev. Lett.* **131**, 036902 (2023).
- [23] Z. Jiang, Z. Liu, Y. Li, and W. Duan, *Phys. Rev. Lett.* **118**, 266401 (2017).
- [24] Z. Jiang, Y. Li, S. Zhang, and W. Duan, *Phys. Rev. B* **98**, 081408(R) (2018).
- [25] Z. Jiang, Y. Li, W. Duan, and S. Zhang, *Phys. Rev. Lett.* **122**, 236402 (2019).

- [26] Z. Jiang, W. Lou, Y. Liu, Y. Li, H. Song, K. Chang, W. Duan, and S. Zhang, *Phys. Rev. Lett.* **124**, 166401 (2020).
- [27] H. Yang, J. Zeng, Y. Shao, Y. Xu, X. Dai, and X.-Z. Li, (2023), [arXiv:2304.00463](https://arxiv.org/abs/2304.00463) [cond-mat.mtrl-sci].
- [28] S. Dong and Y. Li, *Phys. Rev. B* **104**, 085133 (2021).
- [29] S. Dong and Y. Li, *Phys. Rev. B* **107**, 235147 (2023).
- [30] P. E. Blöchl, *Phys. Rev. B* **50**, 17953 (1994).
- [31] G. Kresse and D. Joubert, *Phys. Rev. B* **59**, 1758 (1999).
- [32] G. Kresse and J. Furthmüller, *Computational Materials Science* **6**, 15 (1996).
- [33] G. Kresse and J. Furthmüller, *Phys. Rev. B* **54**, 11169 (1996).
- [34] A. Togo and I. Tanaka, *Scripta Materialia* **108**, 1 (2015).
- [35] J. P. Perdew, K. Burke, and M. Ernzerhof, *Phys. Rev. Lett.* **77**, 3865 (1996).
- [36] F. Tran and P. Blaha, *Phys. Rev. Lett.* **102**, 226401 (2009).
- [37] A. D. Becke and E. R. Johnson, *The Journal of Chemical Physics* **124**, 221101 (2006).
- [38] S. Di Sabatino, A. Molina-Sánchez, P. Romaniello, and D. Sangalli, *Phys. Rev. B* **107**, 115121 (2023).
- [39] T. Yamada and S. Hirata, *The Journal of Chemical Physics* **143**, 114112 (2015), [https://pubs.aip.org/aip/jcp/article-pdf/doi/10.1063/1.4929354/15501308/114112\\_1.online.pdf](https://pubs.aip.org/aip/jcp/article-pdf/doi/10.1063/1.4929354/15501308/114112_1.online.pdf).
- [40] J. Čížek and J. Paldus, *The Journal of Chemical Physics* **47**, 3976 (1967), [https://pubs.aip.org/aip/jcp/article-pdf/47/10/3976/18852526/3976\\_1.online.pdf](https://pubs.aip.org/aip/jcp/article-pdf/47/10/3976/18852526/3976_1.online.pdf).
- [41] R. Seeger and J. A. Pople, *The Journal of Chemical Physics* **66**, 3045 (1977), [https://pubs.aip.org/aip/jcp/article-pdf/66/7/3045/18905393/3045\\_1.online.pdf](https://pubs.aip.org/aip/jcp/article-pdf/66/7/3045/18905393/3045_1.online.pdf).
- [42] D. Sangalli, A. Ferretti, H. Miranda, C. Attaccalite, I. Marri, E. Cannuccia, P. Melo, M. Marsili, F. Paleari, A. Marrazzo, G. Prandini, P. Bonfà, M. O. Atambo, F. Affinito, M. Palumbo, A. Molina-Sánchez, C. Hogan, M. Grüning, D. Varsano, and A. Marini, *Journal of Physics: Condensed Matter* **31**, 325902 (2019).
- [43] A. Marini, C. Hogan, M. Grüning, and D. Varsano, *Computer Physics Communications* **180**, 1392 (2009).
- [44] P. Giannozzi, S. Baroni, N. Bonini, M. Calandra, R. Car, C. Cavazzoni, D. Ceresoli, G. L. Chiarotti, M. Cococcioni, I. Dabo, A. D. Corso, S. de Gironcoli, S. Fabris, G. Fratesi, R. Gebauer, U. Gerstmann, C. Gougoussis, A. Kokalj, M. Lazzeri, L. Martin-Samos, N. Marzari, F. Mauri, R. Mazzarello, S. Paolini, A. Pasquarello, L. Paulatto, C. Sbraccia, S. Scandolo, G. Sclauzero, A. P. Seitsonen, A. Smogunov, P. Umari, and R. M. Wentzcovitch, *Journal of Physics: Condensed Matter* **21**, 395502 (2009).
- [45] F. Bruneval and X. Gonze, *Phys. Rev. B* **78**, 085125 (2008).
- [46] A. Guandalini, P. D'Amico, A. Ferretti, and D. Varsano, *npj Computational Materials* **9**, 44 (2023).
- [47] Z. Guo, D. Yan, H. Sheng, S. Nie, Y. Shi, and Z. Wang, *Phys. Rev. B* **103**, 115145 (2021).
- [48] J. Gao, Q. Wu, C. Persson, and Z. Wang, *Computer Physics Communications* **261**, 107760 (2021).
- [49] R. Zhang, J. Deng, Y. Sun, Z. Fang, Z. Guo, and Z. Wang, *Phys. Rev. Res.* **5**, 023142 (2023).
- [50] Z. Guo, J. Deng, Y. Xie, and Z. Wang, *npj Quantum Materials* **7**, 87 (2022).
- [51] S. Zhang, H. Sheng, Z.-D. Song, C. Liang, Y. Jiang, S. Sun, Q. Wu, H. Weng, Z. Fang, X. Dai, and Z. Wang, *Chinese Physics Letters* **40**, 127101 (2023).
- [52] M. Calandra and F. Mauri, *Phys. Rev. Lett.* **106**, 196406 (2011).
- [53] R. Bianco, M. Calandra, and F. Mauri, *Phys. Rev. B* **92**, 094107 (2015).
- [54] F. Di Salvo, C. Chen, R. Fleming, J. Waszczak, R. Dunn, S. Sunshine, and J. A. Ibers, *Journal of the Less Common Metals* **116**, 51 (1986).
- [55] A. Nakano, T. Hasegawa, S. Tamura, N. Katayama, S. Tsutsui, and H. Sawa, *Phys. Rev. B* **98**, 045139 (2018).
- [56] S. Y. Kim, Y. Kim, C.-J. Kang, E.-S. An, H. K. Kim, M. J. Eom, M. Lee, C. Park, T.-H. Kim, H. C. Choi, B. I. Min, and J. S. Kim, *ACS Nano* **10**, 8888 (2016).
- [57] G. Pizzi, V. Vitale, R. Arita, S. Blügel, F. Freimuth, G. Géranton, M. Gibertini, D. Gresch, C. Johnson, T. Koretsune, J. Ibañez-Azpiroz, H. Lee, J.-M. Lihm, D. Marchand, A. Marrazzo, Y. Mokrousov, J. I. Mustafa, Y. Nohara, Y. Nomura, L. Paulatto, S. Poncé, T. Ponweiser, J. Qiao, F. Thöle, S. S. Tsirkin, M. Wierzbowska, N. Marzari, D. Vanderbilt, I. Souza, A. A. Mostofi, and J. R. Yates, *Journal of Physics: Condensed Matter* **32**, 165902 (2020).
- [58] M. Rohlfing and S. G. Louie, *Phys. Rev. B* **62**, 4927 (2000).
- [59] B. Scharf, G. Xu, A. Matos-Abiague, and I. Žutić, *Phys. Rev. Lett.* **119**, 127403 (2017).
- [60] M. F. C. M. Quintela, J. C. G. Henriques, L. G. M. Tenório, and N. M. R. Peres, *physica status solidi (b)* **259**, 2200097 (2022).
- [61] P. Cudazzo, I. V. Tokatly, and A. Rubio, *Phys. Rev. B* **84**, 085406 (2011).
- [62] H. Yang, X. Wang, and X.-Z. Li, *New Journal of Physics* **24**, 083010 (2022).
- [63] N. Higashihara, Y. Okamoto, Y. Yoshikawa, Y. Yamakawa, H. Takatsu, H. Kageyama, and K. Takenaka, *Journal of the Physical Society of Japan* **90**, 063705 (2021).
- [64] J. Huang, B. Jiang, J. Yao, D. Yan, X. Lei, J. Gao, Z. Guo, F. Jin, Y. Li, Z. Yuan, C. Chai, H. Sheng, M. Pan, F. Chen, J. Liu, S. Gao, G. Qu, B. Liu, Z. Jiang, Z. Liu, Y. Huang, Q. Zhang, S. Li, S. Jin, H. Ding, J. Shen, D. Su, Y. Shi, Z. Wang, and T. Qian, (2023), [arXiv:2312.14455](https://arxiv.org/abs/2312.14455) [cond-mat.mtrl-sci].
- [65] P. Zhang, Y. Dong, D. Yan, B. Jiang, T. Yang, J. Li, Z. Guo, Y. Huang, B. Hao, Q. Li, Y. Li, K. Kurokawa, R. Wang, Y. Nie, M. Hashimoto, D. Lu, W.-H. Jiao, J. Shen, T. Qian, Z. Wang, Y. Shi, and T. Kondo, (2023), [arXiv:2312.14456](https://arxiv.org/abs/2312.14456) [cond-mat.mtrl-sci].
- [66] M. S. Hossain, T. A. Cochran, Y.-X. Jiang, S. Zhang, H. Wu, X. Liu, X. Zheng, B. Kim, G. Cheng, Q. Zhang, M. Litskevich, J. Zhang, Z.-J. Cheng, J. Liu, J.-X. Yin, X. P. Yang, J. Denlinger, M. Tallarida, J. Dai, E. Vescovo, A. Rajapitamahuni, H. Miao, N. Yao, Y. Peng, Y. Yao, Z. Wang, L. Balicas, T. Neupert, and M. Z. Hasan, (2023), [arXiv:2312.15862](https://arxiv.org/abs/2312.15862) [cond-mat.str-el].